Clim. Past Discuss., 7, 635–675, 2011
www.clim-past-discuss.net/7/635/2011/
doi:10.5194/cpd-7-635-2011

Climate of the Past Discussions

Tracking climate variability in the western Mediterranean during the Late Holocene: a multiproxy approach

V. Nieto-Moreno[1], F. Martínez-Ruiz[1], S. Giralt[2], F. Jiménez-Espejo[1], D. Gallego-Torres[3], M. Rodrigo-Gámiz[1], J. García-Orellana[4], M. Ortega-Huertas[5], and G. J. de Lange[3]

[1]Instituto Andaluz de Ciencias de la Tierra (CSIC-UGR), Facultad de Ciencias, Universidad de Granada, Campus Fuentenueva s/n, 18002, Granada, Spain
[2]Institute of Earth Sciences Jaume Almera (CSIC), Lluís Solé i Sabarís s/n, 08028, Barcelona, Spain
[3]Marine Geochemistry and Chemical Oceanography Department, Geosciences Faculty, Utrecht University, 3508, Utrecht, The Netherlands

[4]Departament de Física – Institut de Ciència i Tecnologia Ambientals (ICTA), Universitat Autònoma de Barcelona, 08193, Bellaterra, Spain
[5]Departamento de Mineralogía y Petrología, Facultad de Ciencias, Universidad de Granada, Campus Fuentenueva s/n, 18002, Granada, Spain

Received: 21 January 2011 – Accepted: 16 February 2011 – Published: 21 February 2011

Correspondence to: V. Nieto-Moreno (vanesanieto@ugr.es)

Published by Copernicus Publications on behalf of the European Geosciences Union.

Abstract

Climate variability in the western Mediterranean is reconstructed for the last 4000 yr using marine sediments recovered in the west Algerian-Balearic basin, near the Alboran basin. Fluctuations in chemical and mineralogical sediment composition as well as grain size distribution are linked to fluvial-eolian oscillations, changes in redox conditions and paleocurrent intensity. Multivariate analyses allowed us to characterize three main groups of geochemical and mineralogical proxies determining the sedimentary record of this region. These three statistical groups were applied to reconstruct paleoclimate conditions at high resolution during the Late Holocene. An increase in fluvial-derived elements (Rb/Al, Ba/Al, REE/Al, Si/Al, Ti/Al, Mg/Al and K/Al ratios), finer grain size, slower flows and oxygen-poor bottom waters – as suggested by sortable silt (10–63 µm), clays (< 2 µm) and redox-sensitive elements (V/Al, Cr/Al, Ni/Al and Zn/Al ratios) – depict the Roman Humid Period (RHP) and the Little Ice Age (LIA), while drier environmental conditions are recognized during the Late Bronze Age-Iron Age (LBA-IA) and the Medieval Warm Period (MWP). Although no Ba excess was registered, other paleoproductivity indicators (total organic carbon content, Br/Al ratio, and organometallic ligands such as U and Cu) display the highest values during the RHP, this period exhibiting by far the most intense productivity of the last 4000 yr. These marine sediments evidence oscillations that support the link of the westernmost Mediterranean climate with the North Atlantic coupled ocean-atmosphere climatic system, pointing to solar irradiance and the North Atlantic Oscillation (NAO) variability as the main driving mechanisms behind natural climate variability over decadal to centennial time-scales for the last 4000 yr.

1 Introduction

Although more attention has been classically devoted to major climate changes during the last deglacial period (Younger Dryas, Dansgaard/Oeschger cycles and the last

CPD
7, 635–675, 2011

Heinrich event) (Dansgaard et al., 1993; Magny et al., 2001; Stein et al., 2009), the Holocene has also been punctuated by significant rapid climate variability including polar cooling, aridity, and changes in the intensity of atmospheric circulation (Mayewski et al., 2004; Wanner et al., 2008).

These climatic oscillations have been described in Greenland ice cores (e.g., O'Brien et al., 1995; Dawson et al., 2007), and in North Atlantic (e.g., Bond et al., 1997; Bianchi and McCave, 1999), Mediterranean (e.g., Casford et al., 2001; Rohling et al., 2009), Tropical Atlantic (e.g., deMenocal et al., 2000; Rimbu et al., 2004), and Antarctic deep sea cores (e.g., Masson et al., 2000; Bárcena et al., 2002); as well as in lake sediments (e.g., Magny, 2004; Jones et al., 2006), peat bogs (e.g., Blackford and Chambers, 1995), speleothems (e.g., McDermott et al., 2001; Mangini et al., 2007), fossil pollen (e.g., Willard et al., 2005; Jalut et al., 2009) and tree rings (e.g., Esper et al., 2002; Moberg et al., 2005). Nevertheless, the overall lack of agreement about the worldwide distribution, precise timing, amplitude or cause of these fluctuations (Hughes and Diaz, 1994; Crowley and Lowery, 2000; Broecker, 2001) underlines the need for additional local records to reconstruct climate change.

At hemispheric scales, natural external forcing – including solar irradiance variations and volcanic activity – have been highlighted as the main driving mechanisms of natural climate variability on centennial to millennial time-scales during the Holocene (van Geel et al., 1999; Crowley, 2000; Bond et al., 2001). At regional scales, patterns of natural internal climate variability such as El Niño-Southern Oscillation (ENSO) and the NAO are known to vary over decadal to centennial time-scales (Jones et al., 2001; Turney and Palmer, 2007; Trouet et al., 2009). System response to multiple forcing and internal climate variability is further complicated by positive or negative feedback and non-linear responses, such as an interruption or weakening of the North Atlantic Deep Water (NADW) production rate during abrupt cold events (Bond et al., 1997; Bianchi et al., 1999). Besides the mechanisms underlying these natural climate fluctuations, Bond et al. (1997) describe several pervasive millennial scale North Atlantic cooling events (ice-rafted debris events) underway during the Holocene (with a mean pacing of $\sim$ 1500 yr;

CPD
7, 635–675, 2011

nearly the same as the Dansgaard/Oeschger events during the last glaciation), the LIA being the most recent one.

Evidence of abrupt events at the millennial scale during the last deglacial period have been previously reported in the westernmost Mediterranean (Cacho et al., 1999, 2001; Bout-Roumazeilles et al., 2007), revealing that this region is highly sensitive to climate variability and provides ultra high-resolution records at both centennial and millennial scales. North Atlantic cold events have been the framework of abrupt decreases of paleo-sea surface temperatures and salinities (fresh polar water flowing into the Mediterranean Sea through the Strait of Gibraltar), intensification of north-westerly winds towards the Alboran basin and thus enhanced western Mediterranean Deep Water formation (WMDW) (Cacho et al., 1999; Bárcena et al., 2001; Sierro et al., 2005; Voelker et al., 2006; Frigola et al., 2008; Melki et al., 2009), continental dryness and decline of the forest cover extent (Combourieu-Nebout et al., 2002; Sánchez-Goñi et al., 2002), and higher eolian input from the Saharan region (Moreno et al., 2005; Bout-Roumazeilles et al., 2007). Such findings support the linkage of this region with the North Atlantic coupled ocean-atmosphere system.

Despite the broad and intensive paleoenvironmental research performed in the western Mediterranean during the last few decades, high resolution marine records of the Late Holocene are comparatively scarce. This time interval (the last 4000 yr) is characterized by several climatic fluctuations, the best identified among them being the MWP (Lamb, 1965; Hughes et al., 1994) and the LIA (Bradley and Jones, 1993). In this work we integrate data from two different marine records from the west Algerian-Balearic basin. After high resolution analyses, they are compared with records from the Alboran Sea basin. A multiproxy approach was adopted, featuring statistical characterization of the data sets, major and trace element-content fluctuations, grain size distribution, total organic carbon content and mineral composition of marine sediments. This allowed us to identify and characterize the main climate oscillations and local changes, to further advance our understanding of natural climate variability in the westernmost Mediterranean.

CPD
7, 635–675, 2011

2 Climatological and oceanographic setting

The Mediterranean climate is characterized by warm-hot dry summers and mild-cold wet winters. It is located in a transitional zone between two climate belts: the mid-latitude westerly system and the subtropical high-pressure belt. In winter the subtropical high belt is reduced until reaching its southernmost position, thus allowing incursions of westerly winds that introduce mid-latitude cyclones from the Atlantic Ocean. In addition, the North Sea becomes saturated in moisture, resulting in a low intensity precipitation over the Mediterranean region. In summer, the subtropical high-pressure belt remains over this region, thus restraining precipitation and inducing climate dryness (e.g., Sumner et al., 2001).

At decadal time-scales, the prevailing winter climate variability pattern in the North Atlantic region is the NAO. It is based on fluctuations in the sea-level atmospheric pressure between the Icelandic low and the Azoric high-pressure centres. The positive phase of the NAO is characterized by a stronger than usual subtropical high plus a deeper than normal polar low-pressure centre. This gives rise to pressure difference that are stronger than the average westerlies, tracing a pathway across middle latitudes farther to the north, and leading to dry, cold winters in southern Europe, the Mediterranean, northern Africa, northern Canada and Greenland, and to warm, wet winters in northern Europe and eastern North America.

The negative phase of the NAO is linked to opposite anomalies. Over the past 25 yr, unprecedented strongly-positive NAO phases have been recorded (Hurrell, 1995; Rodó et al., 1997). Prolonged periods of both positive and negative phases of the NAO, alter evaporation-precipitation patterns, melt sea ice, continental runoff, and the rate of deep water formation in the North Atlantic, as proposed for the MWP over Europe (Trouet et al., 2009).

In terms of oceanographic conditions, the Mediterranean Sea is characterized by a general thermohaline circulation driven by excessive evaporation with respect to precipitation and runoff, as determined by the exchange of water that takes place through

CPD
7, 635–675, 2011

the Strait of Gibraltar (Bethoux, 1979). Hence, the Atlantic jet stream becomes saltier and denser when it flows into the Mediterranean Sea (Modified Atlantic Water, MAW; 200–300 m thick); and two anticyclonic gyres are produced when it progresses eastwards to the Algerian Basin (Western and Eastern Alboran Gyres) (Perkins et al., 1990; Millot, 1999).

The Atlantic water entering the Mediterranean Sea is offset by a deep-water outflow (Mediterranean Outflow Water; MOW) consisting of Levantine Intermediate Water (LIW) and WMDW, respectively originating in the Levantine Mediterranean Sea and in the Gulf of Lyon (Kinder and Parrilla, 1987).

3 Paleoenvironmental proxies: the mineralogical and geochemical record in the westernmost Mediterranean

The detrital fraction of deep-sea sediments provides further insight regarding the climate conditions prevailing in source areas and their influence on adjacent landmasses and the mechanisms involved in the transport of material from land to sea (riverine and eolian input), as well as changes in the oceanic and atmospheric circulation that may trigger its dispersion. Therefore, the detrital fraction is held to be a reliable proxy for paleoceanographic and paleoenvironmental reconstructions.

Previous studies of clay mineral composition in the western Mediterranean signal riverine and wind-blown particles as the main sources (Martínez-Ruiz et al., 1999, 2003; Moreno et al., 2005; Bout-Roumazeilles et al., 2007). Illite and smectite are fluvial-derived, whereas kaolinite and additional fibrous clay minerals (palygorskite and/or sepiolite) are considered reworked wind-blown particles from western Morocco and northern Algeria (Bout-Roumazeilles et al., 2007).

Element/Al ratios (such as Rb/Al, Mg/Al, K/Al, Si/Al, Ti/Al and Zr/Al) have also been studied to infer fluctuations in terrestrial run-off, erosional processes and riverine and eolian input to the Alboran basin (Moreno et al., 2005; Jiménez-Espejo et al., 2008). Aluminum-normalization is commonly used to envisage fluctuations in detrital

CPD
7, 635–675, 2011

alumino-silicate source material (e.g., Van der Weijden, 2002). Ba/Al and biogenic barite are widely used as paleoproductivity proxies in the western Mediterranean Sea in relation to episodes of enhanced productivity such as the Heinrich events (Moreno et al., 2004; Jiménez-Espejo et al., 2008). Recently, Martín-Puertas et al. (2010) integrated marine and lacustrine records from the South Iberian region to reconstruct environmental changes during the Late Holocene by using fluvial and eolian input proxies (Mg/Al, Zr/Al).

Meanwhile, redox-sensitive trace elements provide information about changes in bottom water oxygenation. Because their solubility depends on their valence which in turns depends on the prevailing redox conditions, they are useful as paleoredox proxies. Previous research has used these redox-sensitive elements to describe deep-water conditions at the time of deposition in the western Mediterranean (Martínez-Ruiz et al., 2003; Moreno et al., 2004; Jiménez-Espejo et al., 2007; Rogerson et al., 2008).

Approaches to correlate grain size to relative paleocurrent intensity refer to the percentage of sortable silt or coarse silt (SS, 10–63 µm) as a proxy of relative paleocurrent speed. The silt/clay ratio (S/C) supplies further information about deepwater paleocurrent variability (McCave et al., 1995; McCave and Hall, 2006). These proxies have been successfully applied in the western Iberian margin, showing that high SS values and S/C ratios correlate with faster flows and better oxygenated deep waters during dry periods (Hall and McCave, 2000; Moreno et al., 2005; Frigola et al., 2007; Rogerson et al., 2008). Thus, median and mean grain size values and quartz content (%) are also considered in our study to complement the information provided by grain size distribution during the Late Holocene.

4 Materials and methods

Two gravity-cores, 305G (36°23,603′ N, 1°22,710′ W, 2512 m b.s.l.) and 306G (36°27,846′ N, 1°11,166′ W, 2574 m b.s.l) – recovered during the Training-Through-Research Cruise 14 (TTR-14), Leg 2, in the west Algerian-Balearic basin – were

CPD
7, 635–675, 2011

selected for this study (Fig. 1). The sediments mainly consist of water-saturated brownish mud in the upper part, and greyish clay, quite homogeneous but becoming darker downwards, together with foraminifera and some shell fragments (Comas and Ivanov, 2006).

Both cores were sampled in 1 cm thick slices to obtain a high resolution record for the last 4000 yr. Samples were treated to analyze chemical and mineralogical composition using different techniques. Bulk and clay mineral compositions were obtained by X-Ray Diffraction using a PANalytical X'Pert PRO diffractometer with Cu-Kα radiation and automatic slit. Clay fraction separation and sample preparation was performed according to the international recommendations compiled by Kisch (1991). Diffractograms were visually interpreted using Xpowder software (Martin, 2004; http://www.xpowder.com). Peak areas were measured in order to estimate semiquantitative mineral contents, the estimated error being < 5% for bulk mineral composition and 5–10% for clay mineral proportions.

Quantitative geochemical microanalyses every five centimetres for clay mineral characterization were achieved by Transmission Electron Microscopy (HR-TEM; Philips CM-20 provided with and EDAX microanalysis system). Additional morphological analyses of clays, barite and pyrite from selected samples were acquired by Field Emission Scanning Electron Microscopy (FE-SEM; LEO-Carl Zeiss-GEMINI-1530). Barite was separated from eight selected samples with higher Ba content by a sequential leaching procedure (Eagle et al., 2003).

Major elements were measured using Wavelength Dispersive X-Ray Fluorescence Spectrometry (WDXRF; Bruker AXS S4 Pioneer with an Rh anode X-ray tube), using pressed pellets, with an analytical detection limit of 0.1% and an instrumental error < 1%. Trace elements were analyzed by Inductively Coupled Plasma-Mass Spectrometry (ICP-MS; Perkin-Elmer Sciex Elan 5000) using Re and Rh as internal standards with an instrumental error of ±2% and ±5% for elemental concentrations of 50 ppm and 5 ppm, respectively (Bea, 1996). Samples were prepared by sequential acid digestion (HNO_3 + HF) and measured in triplicate.

CPD
7, 635–675, 2011

TOC content was determined using a Horiba EMIA-320V Series Carbon/Sulfur Analyzer. Grounded samples were subjected to acid leaching (HCl) onto glass fiber filters in order to remove inorganic carbon. Treated samples were oxidized by the high-frequency induction furnace method under an oxygen stream, and CO_2 gases evolved were detected by calibrated infra-red (IR) cells. TOC contents were measured as milligrams and calculated as percentages of the sample weight. The accuracy of the method is 92%, and precision is 0.01%.

Grain size was determined as a cumulative mass percentage using a Micromeritic Sedigraph III 5120, which measures particles ranging from 0.10 to 63 µm. Resolution and accuracy are, respectively, 1 and 0.1 µm. A granulometric study was undertaken on the bulk fraction at 2 cm intervals, taking away the coarse fraction (> 63 µm) by wet sieving and removing carbonates and organic matter from the remaining silt (2–63 µm) and clay fraction (< 2 µm) by treatment with acetic acid and hydrogen peroxide (10%), respectively. Two split fractions were established for the terrigenous silt: (a) fine silt (2–10 µm), cohesive, mainly composed of clay minerals and settled as aggregated material, and (b) coarse silt (10–63 µm) or sortable silt (SS), predominantly composed of quartz and feldspar and with non-cohesive behaviour.

Statistical treatment of analytical data was performed using the statistical software package R (R Development Core Team, 2010). Stratigraphically-constrained cluster analyses were applied to identify the main geochemical families and the outliers (isolated samples of anomalous values). The normalized geochemical dataset was also clustered in order to find groups of variables showing similar behaviour. The complete linkage method (or furthest neighbour method) together with the "gclus" package (Hurley, 2009) were used for clustering purposes. Redundancy Analyses (RDA) were carried out on the geochemical and the mineralogical data set using the "vegan" package (Oksanen et al., 2009) to infer the relationship between them, and Principal Component Analyses (PCA) were performed on the geochemical data set to characterize the main underlying gradients governing the sedimentary environment.

CPD
7, 635–675, 2011

5 Age-depth model and sedimentation rate

The age-depth model is based on five ^{14}C-AMS dates for each core performed on monospecific planktonic foraminifera (*Globigerina Bulloides)* extracted from the > 125 µm fraction and analyzed by Accelerator Mass Spectrometry (National Centre for Accelerators, CNA Spain, and Poznan Radiocarbon Laboratory, Poland). Radiocarbon ages were calibrated to calendar years (cal. BP) using the CALIB 6.0 software (Stuiver and Reimer, 1993) and the MARINE09 curve (Reimer et al., 2009), assuming a marine reservoir age correction of 400 yr. Conventional and calibrated radiocarbon ages are reported in Table 1. In order to obtain an age-depth model, a linear interpolation was applied between dates, giving mean sedimentation rates of 10.2 and 10.7 cm kyr^{-1} for cores 305G and 306G, respectively. ^{210}Pb was determined in the first five centimetres of both cores to obtain the most recent sedimentation rates. Results showed that ^{210}Pb was in excess only in the two first centimetres. Comparing the determined ^{210}Pb inventory (around 1000 Bq m^{-2} for both cores) with other sediment records from the area (Masqué et al., 2003), a loss of the surface part of the sediment during the gravity core recovery was detected. Although some surface sediment loss is expected due to gravity core recovery, the enrichment of ^{210}Pb in the first centimetre and the exponential decrease of ^{210}Pb concentrations observed in both cores suggest that the age of the topmost part is around 150 yr in both cores, which is in agreement with the age inferred from ^{14}C-AMS dates.

6 Statistical analyses: Grouping proxies for paleoclimatic reconstruction

The identification and characterization of the main processes leading the sedimentary deposition in the study area was based on statistical analyses of the mineralogical and geochemical data sets. Normalized matrix clustering of the geochemical data (Fig. 2a and b) allowed us to identify the main geochemical families showing similar behaviour, and thus a high correlation in terms of their affinity and origin. RDA biplots illustrate

CPD
7, 635–675, 2011

the relationships between the chemical elements and their associated mineral phases. Three main groups in accordance with their origin in both sites were defined (Fig. 2c and d).

The first group comprises fluvial (illite, feldspars, smectite, dolomite, Al, Th, Rb, Ba, REE, Mg, K, Fe, Si and Ti) and eolian (kaolinite, Zr) derived element/minerals (Fig. 2a, b, c and d). Quartz appears between detrital proxies of fluvial and eolian provenance, which suggests that it could come from both sources (Kolla et al., 1979) (Fig. 2c and d). Ba is included in this first group, and its association with alumino-silicates points to a detrital origin. Si and Ti have multiple hosts in marine sediments that vary considerably in particle size, ranging from clay to heavy minerals such as quartz or accessory Ti-bearing heavy minerals (Kolla et al., 1979; Calvert and Fontugne, 2001). Cluster and RDA analyses bound both elements to aluminium, thus revealing clay minerals as the most important hosts and riverine input as the main supply to the basin. REE show a high statistical significance with this detrital group in both cases (for cores 305G and 306G, respectively Th: $r^2 = 0.89$ and 0.96, $p < 0.01$; Ba: $r^2 = 0.79$ and 0.96, $p < 0.01$) (Fig. 2a and b), thus also revealing clay minerals as the most important hosts, while Rb is closely linked to K and to clay minerals (Horstman, 1957). The second group is composed of redox-sensitive elements including two sub-groups: those which are less soluble under reducing conditions and provide information on water oxygenation conditions (V, Cr, Ni, Zn), and those constituting insoluble oxy-hydroxides under oxic conditions (Mn) and elements easily captured into them (Co, Mo). This second group is associated with the detrital one, pointing to alumino-silicates as main hosts. The third group contains paleoproductivity indicators associated with the organic flux, showing the high correlation between Br and marine organic matter, probably due to favoured uptake of bromine from seawater by marine plants (ten Haven et al., 1988; Ziegler et al., 2008). This provides a semiquantitave estimation of sedimentary organic matter. Although U and Cu are often used as redox-sensitive elements, cluster analyses show them to be associated to the cluster containing organic carbon and carbonates.

CPD
7, 635–675, 2011

The first two eigenvectors of the PCA account for 70% and 73% of the total variance at sites 305G and 306G, respectively. The first eigenvector represents 47% and 57% of the total variance at sites 305G and 306G, respectively, and is mainly controlled by the detrital-productivity groups, whereas the second eigenvector represents 23% and 16% of the total variance and is mainly triggered by the water oxygenation conditions (Fig. 2e and f). This is most likely due to the slightly different location in the basin; site 305G is closer to the continental slope and thus at the base of the canyon discharge, while site 306G is more distal (Fig. 1).

In light of these results, we applied the geochemical and mineralogical set of identified proxies to reconstruct detrital input oscillations, oxygenation conditions, paleoproductivity and post-depositional alteration during the last 4000 yr in the western Mediterranean.

7 Mineral composition, detrital input and grain size distribution

The analyzed sediments (cores 305G and 306G) are predominantly composed of clay minerals (30–70%), calcite (20–45%) and quartz (10–30%), with minor amounts of dolomite and feldspars (< 10%). Clay mineral assemblages consist of detrital mica (50–90%), kaolinite + chlorite (5–40%) and smectites (< 20%). Additional fibrous clay minerals, such as palygorskite and sepiolite, were also identified using Transmission Electron Microscopy. These analyses verify that smectite composition corresponds to a beidellites-type of detrital origin, aluminium-enriched and soil-derived.

At both sites, Rb/Al, Ba/Al, Si/Al, Ti/Al, Mg/Al, and K/Al ratios show a similar general profile with slight differences (Fig. 3). Both cores exhibit a decreasing trend during the LBA-IA, the so-called Dark Ages (DA, transition between the RHP and the MWP; ~ 1600–1150 cal. yr BP) and the MWP, the trend less evident in the case of Mg/Al and K/Al ratios at site 306G during the LBA-IA. An increase in these ratios is observed during the late RHP, DA and LIA. The Zr/Al ratio gives relatively high values in the early LBA-IA and MWP and low values during the RHP and the LIA. The lowest values are

CPD
7, 635–675, 2011

reached in the middle RHP, DA and the LIA, and the highest in the late RHP and the MWP.

The mean grain size at sites 305G and 306G ranges between 1–8 and 0.5–10 µm, and respective median grain size is < 2 and 4 µm (Fig. 4). The grain size distribution is therefore mainly composed of clays and fine silts. Clays are most abundant at site 306G and fine silt in the case of site 305G. This fits well with the slightly different location mentioned above, with respect to the continental slope or the canyon base (Fig. 1). Regarding SS values, a parallel trend is observed at both sites, the peaks coinciding with increasing trends of the mean and the median distributions and the quartz content. These coarser sediments occur at the end of the LBA-IA and the beginning of the RHP (~ 2800–2200 cal. yr BP), and during the MWP and the first half of the LIA (~ 1400–400 cal. yr BP).

8 Paleoproductivity indicators, oxygen conditions and post-depositional alteration

TOC values are below 1% at both sites (Fig. 5). Although the general profile exhibits a progressive down-core decline, both cores display the highest values during the RHP and at the top in both cases. Br/Al ratio mainly mirrors the TOC content trend, achieving maximum values during the RHP and at the top of the core. U/Th displays a flat pattern at both sites except during the RHP, when this ratio increases and maximum values are reached. The increase concludes at the beginning of the MWP at site 306G. Although Cu/Al ratios display more erratic behaviour, it is possible to discern two Cu/Al enhancements during the RHP, one in each core.

At site 305G, the V/Al, Cr/Al, Ni/Al and Zn/Al ratios (Fig. 6) draw a declining trend during the LBA-IA and the MWP, reaching the lowest values during the LBA-IA. Values rise progressively during the first half of the RHP and the whole LIA, then decrease sharply around 1800 cal. yr BP and remain low throughout the DA. A similar evolution is seen at site 306G, with the exception of the LBA-IA, when these ratios increase.

CPD
7, 635–675, 2011

Minimum values are reached during the MWP, and an abrupt decrease likewise takes place around 1800 cal. yr BP.

Both sites display a flat post-depositional pattern of Mn/Al except for sudden increases from 1350 until 600 cal. yr BP for site 305G, and between 1750–1350 cal. yr BP and 900–450 cal. yr BP for site 306G (Fig. 7), evidencing a post-depositional oxidation. Mn and Fe enrichments and early oxidation of organic matter above the redoxcline point to the typical boundary on oxic/suboxic pelagic sediments reported in Eastern Mediterranean sapropels and in uppermost hemipelagic sediments in the western Mediterranean (Thomson et al., 1999; Masqué et al., 2003). Fe/Al enrichments also occur subsequent to Mn peaks, from 1700 until 1200 cal. yr BP at site 305G; yet a double peak is seen for site 306G, between 2050–1700 cal. yr BP and 1650–1300 cal. yr BP. Both precipitate as oxy-hydroxides (Fig. 7). Co/Al and Mo/Al are also enriched in the post-depositional oxidation front at both sites, most likely co-precipitated with Fe and Mn oxy-hydroxides (Fig. 7). This front is also responsible for organic matter oxidation, as supported by the lower values and decreasing trend of TOC (Fig. 5).

9 Paleoclimate conditions

9.1 Late Bronze Age-Iron Age (LBA-IA) (~ 3600–2600 cal. yr BP)

A decreasing trend of fluvial derived-elements took place from ~ 3500 cal. yr BP until ~2800 cal. yr BP at both sites (Fig. 3), coinciding with the North Atlantic cold event 2 (~ 2800 cal. yr BP) (Bond et al., 1997) and a decline in solar irradiance at the hemispheric mean scale (~ 3500–2500 cal. yr BP) (Mayewski et al., 2004). This would suggest a riverine input decline into the basin and subsequent dryness. The Zr/Al ratio, associated to Saharan eolian input fluctuations, draws relatively high values in the early LBA, with a general decreasing trend in the RHP. These decreasing trends at both sites coincide with a progressive evolution towards typical Mediterranean climate and aridity, which gradually occurs from the beginning of the middle Holocene (Neoglacial phase,

CPD
7, 635–675, 2011

~ 5000 cal. yr BP) owing to an orbitally-induced decline of summer insolation in the Northern Hemisphere (Wanner et al., 2008).

The deposition of coarser grain size sediments, higher quartz content and reduced redox-sensitive trace element values at site 305G (Figs. 4 and 6) also supports this dryness, suggesting higher energetic hydrodynamic bottom conditions, and thus, faster flows and better oxygenated bottom waters. However, at site 306G, Mg/Al and K/Al ratios rise, grain size and quartz content decrease, and redox-sensitive trace element values increase. Local reasons could be invoked to explain this disagreement. Their slightly different locations with respect to the continental slope and the base of the canyons expose these sites to different sedimentary processes (Fig. 1). Regarding marine paleo-productivity, low TOC values as well as Cu/Al, Br/Al and U/Th ratios suggest lower organic matter preservation and better oxygenated bottom sediments (Fig. 5).

Furthermore, dry conditions have been described in the western Mediterranean region based on marine and terrestrial pollen records (Jalut et al., 2000, 2009; Combourieu-Nebout et al., 2009). Reduced river activity in Southern Europe (Magny et al., 2002; Macklin et al., 2006), cooling events with lower temperatures and faster flows in the Balearic basin (Frigola et al., 2007), and a desiccation phase in a lacustrine record from Southern Spain (Carrión, 2002) are likewise reported for this time frame. Martín-Puertas et al. (2010) recorded a dry period supported by higher Saharan input into the Alboran basin (Zr/Al ratio; core 300G) during this period. In contrast, higher lake levels have been observed in Jura and French subalpine ranges (mid-Europe) (Magny, 2004). Although these records show a common underlying climatic pattern in the westernmost Mediterranean, lacustrine systems in mid-Europe might have been exposed to the influence of a different regional climatic pattern.

9.2 The Roman Humid Period (RHP) (~ 2600–1600 cal. yr BP)

The early and middle RHP (~ 2600–1800 cal. yr BP) is marked by a decreasing trend in eolian input at both sites (Zr/Al, Fig. 3), pointing to an ongoing establishment of

CPD
7, 635–675, 2011

more humid conditions in the western Mediterranean. The decrease of fluvial derived-elements that took place during the LBA became a relatively steady pattern during this period, leading to a progressive establishment of wetter conditions. This climate framework is also suggested by the progressively finer grain size and lower quartz content (Fig. 4), slightly increased values of redox sensitive elements (Fig. 6) and a sudden increase in TOC values and organometallic ligands (Fig. 5), indicating slower and less energetic flows, and decreasing oxygenation bottom conditions.

Other records in this region support this scenario during the early and the middle RHP. Accordingly, dry conditions are described for pollen (Jalut et al., 2000, 2009; Combourieu-Nebout et al., 2009), marine (Frigola et al., 2007; Combourieu-Nebout et al., 2009), lacustrine (Carrión, 2002), and fluvial records (Magny et al., 2002; Macklin et al., 2006) in the western Mediterranean. Humid conditions are observed in lacustrine records at this time interval in the Jura and French subalpine ranges, however (Magny, 2004).

The most noteworthy event coinciding with the RHP is the sudden rise in fluvial land-derived elements that occurred at the end of the RHP, around 1800 cal. yr BP at both sites. This could derive into a sharp nutrient flux as reflected by paleo-productivity indicators and associated ratios (Fig. 5), thus defining this period as the most intense productivity and humid by far of the last 4000 yr. Such an influx of fresh water from a large flood may have enhanced stratification of the water column, in turn increasing organic matter preservation. Indeed, finer grain size and slightly raised values of redox sensitive elements suggest slower deep water flows and decreased oxygen bottom conditions (Figs. 4 and 6). The Zr/Al ratio remains low after 1800 cal. yr BP, though a slight rise in the trend points to drier conditions after the maximum fluvial input achieved around 1600 cal. yr BP.

Flooding events in the Iberian Peninsula are also recorded for this time (Macklin et al., 2006), as are higher lake levels in mid-Europe (Magny, 2004). Martín-Puertas et al. (2010) describe wetter conditions sharpening at 1700 cal. yr BP in the Alboran basin during the RHP (Mg/Al ratio; ODP 976) and decreased eolian input from the African

CPD
7, 635–675, 2011

margin (Zr/Al ratio; core 300G), to characterize this period as the most humid of the Late Holocene.

9.3 The Medieval Warm Period (MWP) (~ 1150–650 cal. yr BP)

The transition between the RHP and the MWP, the DA, can be characterized by a progressive dryness sharpening around 1300 cal. yr BP at both sites, which coincides with the North Atlantic cold event 1 (~ 1400 cal. yr BP) (Bond et al., 1997). This fact is revealed by a decline of riverine influence to the basin (Fig. 3), enhanced sortable silt and quartz content that would evoke higher speed bottom currents and energetic hydrodynamic conditions (Fig. 4), and better oxygenated bottom waters, denoted by decreasing redox-sensitive elements (Fig. 6). Subsequent to this decline, an abrupt increase of fluvial derived-elements takes place, which is not reflected by Mg/Al and K/Al. The fact that there are no apparent fluctuations of the other proxies suggests this might be due to a size sorting effect of the heavier elements. Regarding marine paleo-productivity, lower TOC values as well as Cu/Al, Br/Al and U/Th ratios indicate poor organic matter preservation due to the lower terrestrial land derived-influx and well-oxygenated bottom sediments (Fig. 5). However, at site 306G, the U/Th ratio sustains high values until the beginning of the MWP, very likely due to the association of this element with an inorganic phase. The Zr/Al ratio suggests a progressive sharp dryness from 2000 cal. yr BP until the beginning of the MWP when the highest values are reached, before the Medieval solar activity maximum (~ 850–700 cal. yr BP) (Jirikowic and Damon, 1994). Afterwards, a steady decline takes place throughout the MWP (Fig. 3).

The dryness that characterizes the DA is correlated with a decrease in humidity in the western Mediterranean evidenced by forest cover regression episodes (Jalut et al., 2000, 2009; Combourieu-Nebout et al., 2009), a decrease in river activity in southern Europe (Magny et al., 2002; Macklin et al., 2006), cooling events in the Balearic basin (Frigola et al., 2007), and lower lake levels in southern Spain (Carrión, 2002). In

CPD
7, 635–675, 2011

contrast, higher lake levels have been evidenced in Jura and French subalpine ranges (mid-Europe) (Magny, 2004).

During the MWP, a decline of fluvial-derived elements takes place together with an increase in grain size and quartz content and a decrease in redox-sensitive elements, pointing to drier conditions that are accentuated during the Medieval solar activity maximum. This period coincides with an aridification phase due to a decline in solar irradiance (1200–1000 cal. yr BP) (Mayewski et al., 2004). This phase has been evidenced in the Mediterranean region through changes in vegetation (Jalut et al., 2000, 2009; Combourieu-Nebout et al., 2009), and a decrease in river activity in southern Europe (Magny et al., 2002; Macklin et al., 2006). Drier conditions were recorded during the MWP, characterized by a decrease of the riverine input into the Alboran basin (Mg/Al ratio, 976 ODP) (Martín-Puertas et al., 2010).

9.4 The Little Ice Age (LIA) (~ 650–150 cal. yr BP)

The drier conditions recognized during the MWP are maintained during the first half of the LIA until 400 cal. yr BP. Martín-Puertas et al. (2010) also recorded a decrease of riverine input during the LIA, reaching even lower values than during the MWP. Further records in the western Mediterranean mirror these conditions. Thus, Carrión (2002) recorded a desiccation phase in a lacustrine record from Southern Spain, and Frigola et al. (2007) described cooling events in the Balearic basin at this time, although Magny (2004) showed higher lake levels in mid-Europe at this time.

A rise in fluvial land-derived elements (Fig. 3), decreasing grain size and lower quartz content (Fig. 4), and higher values for redox sensitive elements (Fig. 6), TOC values and organometallic ligands (Fig. 7) depict the late LIA. Accordingly, enhanced fresh water input, slower flows, reducing oxygen bottom conditions, better organic matter preservation and thus an establishment of wetter conditions in the western Mediterranean can be envisaged after 400 cal. yr BP to present day time. The typical Saharan eolian input ratio (Zr/Al ratio) draws a declining trend, reaching the lowest values during the last 4000 yr as well as in the RHP (Fig. 3).

CPD
7, 635–675, 2011

This trend correlates with one of the six periods of significant rapid climate change in the Northern Hemisphere due to a decline in solar irradiance (~ 600–150 cal. yr BP) (Mayewski et al., 2004). A slight increase in the riverine input in the Alboran Sea basin is evidenced in the western Mediterranean (Martín-Puertas et al., 2010) and higher lake levels in mid-Europe (Magny, 2004) are seen during the late LIA.

10 Forcing mechanisms driving natural climate variability during the Late Holocene

Solar irradiance variations have been invoked as one of the main forcing mechanisms that drive natural climate variability on centennial to millennial time-scales during the Holocene at the hemispheric scale (van Geel et al., 1999; Crowley, 2000; Bond et al., 2001). At millennial scales, times of orbitally-induced declines of solar irradiance in the Northern Hemisphere might have triggered massive ice sheet collapses and ice-rafted debris discharges that led to a southward advection of cooler and fresher surface water into the North Atlantic current, thus reducing the NADW production rate, and weakening the global thermohaline circulation that could allow these cold pole waters to spread into the Mediterranean Sea through the Strait of Gibraltar. Such events also correlate with an intensification of the atmospheric circulation over Greenland, producing stronger than normal northerly winds that could promote a strengthening of the WMDW production rate and thus of the Mediterranean thermohaline circulation (O'Brien et al., 1995; van Geel et al., 1999; Bond et al., 2001). These millennial-scale abrupt cooling events occur with a mean pacing of 1500 yr during the Holocene, similar to the duration of Dansgaard/Oeschger events that took place during the last deglacial period in the Alboran Sea basin (e.g., Cacho et al., 1999).

Since detrital input is the main process managing deposition at site 305G and 306G, we have selected the first eigenvector of these sites to compare with total solar irradiance (TSI) variations ($W\,m^{-2}$) over the last 4000 yr (Fig. 8) (Steinhilber et al., 2009). A 30-year running average of the TSI variations was plotted to make interpretations visually easier. Thus, TSI positive values are achieved during the RHP and the MWP,

CPD
7, 635–675, 2011

whereas negative values are attained during the LBA-IA, the DA and the LIA. Three minimum negative values are reached during the whole record, two of them coinciding with the North Atlantic cold events described by Bond et al. (1997) (1400 and 2800 cal. yr BP) and the other one taking place during the LIA. These cold imprints in the TSI variations are mirrored at sites 305G and 306G by decreased fluvial input as discussed above (Fig. 3). On the other hand, positive values of the first eigenvector in both cores are seen during the RHP and the LIA, and negative values are achieved during the LBA-IA, DA and the MWP.

The lack of correlation throughout the MWP and the LIA in terms of total solar variations suggests some additional regional force affected detrital input in the western Mediterranean. The NAO, which mainly controls winter precipitation in the North Atlantic region at decadal scales, could be responsible for the regional climate variability. Positive NAO phases in the Mediterranean region are linked with warmer and wetter winters over northern Europe and colder and drier winters over southern Europe as well as northern Africa; opposite patterns of temperature and precipitation are found during negative NAO phases (Wanner et al., 2001; Trigo et al., 2002). Enhanced dust transport from the Sahara region to the North Atlantic Ocean and the Mediterranean Sea has been evidenced during positive NAO phases (Moulin et al., 1997). Furthermore, strongly-positive NAO phases for the MWP and negatives ones for the LIA have been described over Europe (Trouet et al., 2009). At sites 305G and 306G, higher values of Saharan eolian dust input (Fig. 3) and a declining trend in fluvial input (Figs. 3 and 8) take place during the MWP, while opposing trends are recognized during the LIA. Hence, these records further support the NAO as a regional mechanism driving natural climate variability together with the TSI in the western Mediterranean during the Late Holocene, and also sustain the link of the Mediterranean climate with the North Atlantic coupled ocean-atmosphere climate system at centennial and millennial scales during the last 4000 yr.

CPD
7, 635–675, 2011

11 Conclusions

Fluctuations in chemical and mineralogical composition as well as grain size distribution in two deep-sea marine records from the western Mediterranean Sea reveal climate oscillations during the last 4000 yr. These records provide further insight into the response of this highly sensitive area to internal climate variability, allowing for the identification and characterization of humid (LIA and RHP) and dry (MWP and LBA-IA) periods. An increase in fluvial-derived detrital elements (Rb/Al, Ba/Al, REE/Al, Si/Al, Ti/Al, Mg/Al and K/Al ratios), finer grain size (sortable silt), oxygen-poor bottom waters (V/Al, Cr/Al, Ni/Al and Zn/Al ratios), and well preserved marine organic matter (TOC content and Br/Al ratio, U and Cu as organometallic ligands) characterize the RHP and the LIA, whereas essentially opposite paleoenvironmental conditions are recognized during the LBA-IA and the MWP. Likewise, the highest TOC values achieved during the late RHP and the LIA point to this time period as by far the most intense productivity and humid of the last 4000 yr. The correlation of abrupt climatic oscillations with other western Mediterranean records, North Atlantic Cold events and major periods of rapid climate change (RCC) during the Holocene in the Northern Hemisphere comes to support the link between the Mediterranean climate and the North Atlantic coupled ocean-atmosphere climate system. Comparison of the first eigenvector at site 305G and 306G, which represents the detrital input into the basin, with natural external forcing mechanisms of climate variability (as the TSI and the NAO), would underline the TSI as one of the main mechanisms behind natural climate variability on millennial scales. Further influential sources are the modulation of the NAO, a regional prevailing pattern of winter climate variability in the North Atlantic region, and driving natural climate variability on decadal to centennial scales during the MWP and the LIA in the western Mediterranean.

CPD
7, 635–675, 2011

Acknowledgements. This work was financed by Projects CGL2009-07603, CTM2009-07715, 200800050084447 (MARM), Project RNM 05212 and Research Group 0179 (Junta de Andalucía) and Training-Through-Research Programme. We are grateful to CSD2006-00041 (TOPOIBERIA) and CSD2007-00067 (GRACCIE) projects, and Centre for Scientific Instrumentation (CIC-UGR), National Centre for Accelerators (Seville, Spain), Poznan Radiocarbon Laboratory (Poland), Andalusian Institute of Earth Sciences (CSIC-UGR) and Department of Mineralogy and Petrology for the analyses. We are likewise grateful to Alpiste for providing the maps, R. Corral, D. Ortega, E. Holanda, C. Niembro, L. González, E. Abarca and J. Santamarina, as well as the CIC personnel for their laboratory assistance.

References

Bárcena, M. A., Cacho, I., Abrantes, F., Sierro, F. J., Grimalt, J. O., and Flores, J. A.: Paleoproductivity variations related to climatic conditions in the Alboran Sea (western Mediterranean) during the last glacial-interglacial transition: the diatom record, Palaeogeogr., Palaeoclimatol., Palaeoecol., 167, 337–357, doi:10.1016/S0031-0182(00)00246-7, 2001.

Bárcena, M. A., Isla, E., Plaza, A., Flores, J. A., Sierro, F. J., Masqué, P., Sanchez-Cabeza, J. A., and Palanques, A.: Bioaccumulation record and paleoclimatic significance in the Western Bransfield Strait. The last 2000 years, Deep Sea Res. (II Top. Stud. Oceanogr.), 49, 935–950, doi:10.1016/S0967-0645(01)00132-1, 2002.

Bea, F.: Residence of REE, Y, Th and U in granites and crustal protoliths; implications for the chemistry of crustal melts, J. Petrol., 37, 521–552, doi:10.1093/petrology/37.3.521, 1996.

Bethoux, J. P.: Budgets of the Mediterranean Sea: their dependance on the local climate and on the characteristics of the Atlantic waters, Oceanol. Acta, 2, 157–163, 1979.

Bianchi, G. G. and McCave, I. N.: Holocene periodicity in North Atlantic climate and deep-ocean flow south of Iceland, Nature, 397, 515–517, doi:10.1038/17362, 1999.

Blackford, J. J. and Chambers, F. M.: Proxy climate record for the last 1000 years from Irish blanket peat and a possible link to solar variability, Earth Planet. Sc. Lett., 133, 145–150, doi:10.1016/0012-821X(95)00072-K, 1995.

Bond, G., Showers, W., Cheseby, M., Lotti, R., Almasi, P., deMenocal, P., Priore, P., Cullen, H.,

CPD
7, 635–675, 2011

Hajdas, I., and Bonani, G.: A pervasive millennial-scale cycle in North Atlantic Holocene and Glacial climates, Science, 278, 1257–1266, doi:10.1126/science.278.5341.1257, 1997.
Bond, G., Kromer, B., Beer, J., Muscheler, R., Evans, M. N., Showers, W., Hoffmann, S., Lotti-Bond, R., Hajdas, I., and Bonani, G.: Persistent solar influence on North Atlantic climate during the Holocene, Science, 294, 2130–2136, doi:10.1126/science.1065680, 2001.
Bout-Roumazeilles, V., Combourieu Nebout, N., Peyron, O., Cortijo, E., Landais, A., and Masson-Delmotte, V.: Connection between South Mediterranean climate and North African atmospheric circulation during the last 50 000 yr BP North Atlantic cold events, Quaternary Sci. Rev., 26, 3197–3215, doi:10.1016/j.quascirev.2007.07.015, 2007.
Bradley, R. S. and Jones, P. D.: "Little Ice Age" summer temperature variations: their nature and relevance to recent global warming trends, Holocene, 3, 367–376, doi:10.1177/095968369300300409, 1993.
Broecker, W. S.: Was the Medieval Warm Period global?, Science, 291, 1497–1499, doi:10.1126/science.291.5508.1497, 2001.
Cacho, I., Grimalt, J. O., Pelejero, C., Canals, M., Sierro, F. J., Flores, J. A., and Shackleton, N.: Dansgaard-Oeschger and Heinrich event imprints in Alboran Sea paleotemperatures, Paleoceanography, 14, 698–705, doi:10.1029/1999PA900044, 1999.
Cacho, I., Grimalt, J. O., Canals, M., Sbaffi, L., Shackleton, N. J., Schönfeld, J., and Zahn, R.: Variability of the western Mediterranean Sea surface temperature during the last 25 000 years and its connection with the Northern Hemisphere climatic changes, Paleoceanography, 16, 40–52, doi:10.1029/2000pa000502, 2001.
Calvert, S. E. and Fontugne, M. R.: On the late Pleistocene-Holocene sapropel record of climatic and oceanographic variability in the eastern Mediterranean, Paleoceanography, 16, 78–94, doi:10.1029/1999pa000488, 2001.
Carrión, J. S.: Patterns and processes of Late Quaternary environmental change in a montane region of southwestern Europe, Quaternary Sci. Rev., 21, 2047–2066, doi:10.1016/S0277-3791(02)00010-0, 2002.
Casford, J. S. L., Abu-Zied, R., Rohling, E. J., Cooke, S., Boessenkool, K. P., Brinkhuis, H., De Vries, C., Wefer, G., Geraga, M., Papatheodorou, G., Croudace, I., Thomson, J., and Lykousis, V.: Mediterranean climate variability during the Holocene, Mediterr. Mar. Sci., 2, 45–55, 2001.
Comas, M. C. and Ivanov, M. K.: Eastern Alboran margin: the transition between the Alboran and the Balearic-Algerian basins, in: Interdisciplinary geoscience studies of the Gulf of Cadiz

CPD
7, 635–675, 2011

and Western Mediterranean basins, edited by: Kenyon, N. H., Ivanov, M. K., Akhmetzhanov, A. M., and Kozlova, E. V., IOC Technical Series No. 70, UNESCO, 48–61, 2006.
Combourieu-Nebout, N., Turon, J. L., Zahn, R., Capotondi, L., Londeix, L., and Pahnke, K.: Enhanced aridity and atmospheric high-pressure stability over the western Mediterranean during the North Atlantic cold events of the past 50 k.y, Geology, 30, 863–866, doi:10.1130/0091-7613(2002)030¡0863:EAAAHP¿2.0.CO;2, 2002.
Combourieu Nebout, N., Peyron, O., Dormoy, I., Desprat, S., Beaudouin, C., Kotthoff, U., and Marret, F.: Rapid climatic variability in the west Mediterranean during the last 25 000 years from high resolution pollen data, Clim. Past, 5, 503–521, doi:10.5194/cp-5-503-2009, 2009.
Crowley, T. J.: Causes of climate change over the past 1000 years, Science, 289, 270–277, doi:10.1126/science.289.5477.270, 2000.
Crowley, T. J. and Lowery, T. S.: How warm was the Medieval Warm Period?, AMBIO: A Journal of the Human Environment, 29, 51–54, doi:10.1579/0044-7447-29.1.51, 2000.
Dansgaard, W., Johnsen, S. J., Clausen, H. B., Dahl-Jensen, D., Gundestrup, N. S., Hammer, C. U., Hvidberg, C. S., Steffensen, J. P., Sveinbjornsdottir, A. E., Jouzel, J., and Bond, G.: Evidence for general instability of past climate from a 250-kyr ice-core record, Nature, 364, 218–220, doi:10.1038/364218a0, 1993.
Dawson, A. G., Hickey, K., Mayewski, P. A., and Nesje, A.: Greenland (GISP2) ice core and historical indicators of complex North Atlantic climate changes during the fourteenth century, Holocene, 17, 427–434, doi:10.1177/0959683607077010, 2007.
deMenocal, P., Ortiz, J., Guilderson, T., Adkins, J., Sarnthein, M., Baker, L., and Yarusinsky, M.: Abrupt onset and termination of the African Humid Period: rapid climate responses to gradual insolation forcing, Quaternary Sci. Rev., 19, 347–361, doi:10.1016/S0277-3791(99)00081-5, 2000.
Eagle, M., Paytan, A., Arrigo, K. R., van Dijken, G., and Murray, R. W.: A comparison between excess barium and barite as indicators of carbon export, Paleoceanography, 18, 1021, doi:10.1029/2002pa000793, 2003.
Esper, J., Cook, E. R., and Schweingruber, F. H.: Low-frequency signals in long tree-ring chronologies for reconstructing past temperature variability, Science, 295, 2250–2253, doi:10.1126/science.1066208, 2002.
Frigola, J., Moreno, A., Cacho, I., Canals, M., Sierro, F. J., Flores, J. A., Grimalt, J. O., Hodell, D. A., and Curtis, J. H.: Holocene climate variability in the western Mediterranean region from a deepwater sediment record, Paleoceanography, 22, PA2209, doi:10.1029/2006pa001307,

CPD
7, 635–675, 2011

2007.
Frigola, J., Moreno, A., Cacho, I., Canals, M., Sierro, F. J., Flores, J. A., and Grimalt, J. O.: Evidence of abrupt changes in Western Mediterranean Deep Water circulation during the last 50 kyr: A high-resolution marine record from the Balearic Sea, Quatern. Int., 181, 88–104, doi:10.1016/j.quaint.2007.06.016, 2008.
Hall, I. R. and McCave, I. N.: Palaeocurrent reconstruction, sediment and thorium focussing on the Iberian margin over the last 140 ka, Earth Planet. Sc. Lett., 178, 151–164, doi:10.1016/S0012-821X(00)00068-6, 2000.
Horstman, E. L.: The distribution of lithium, rubidium and caesium in igneous and sedimentary rocks, Geochim. Cosmochim. Acta, 12, 1–28, doi:10.1016/0016-7037(57)90014-5, 1957.
Hughes, M. K. and Diaz, H. F.: Was there a "Medieval Warm Period", and if so, where and when?, Clim. Change, 26, 109–142, doi:10.1007/BF01092410, 1994.
Hurley, C.: Gclus: Clustering Graphics, available at:http://cran.r-project.org/package=vegan (last access: January 2011), R package version 1.2, 2009.
Hurrell, J. W.: Decadal trends in the North Atlantic Oscillation: Regional temperatures and precipitation, Science, 269, 676–679, doi:10.1126/science.269.5224.676, 1995.
Jalut, G., Esteban Amat, A., Bonnet, L., Gauquelin, T., and Fontugne, M.: Holocene climatic changes in the Western Mediterranean, from south-east France to south-east Spain, Palaeogeogr., Palaeoclimatol., Palaeoecol., 160, 255–290, doi:10.1016/S0031-0182(00)00075-4, 2000.
Jalut, G., Dedoubat, J. J., Fontugne, M., and Otto, T.: Holocene circum-Mediterranean vegetation changes: Climate forcing and human impact, Quatern. Int., 200, 4–18, doi:10.1016/j.quaint.2008.03.012, 2009.
Jiménez-Espejo, F. J., Martinez-Ruiz, F., Sakamoto, T., Iijima, K., Gallego-Torres, D., and Harada, N.: Paleoenvironmental changes in the western Mediterranean since the last glacial maximum: High resolution multiproxy record from the Algero-Balearic basin, Palaeogeogr., Palaeoclimatol., Palaeoecol., 246, 292–306, doi:10.1016/j.palaeo.2006.10.005, 2007.
Jiménez-Espejo, F. J., Martínez-Ruiz, F., Rogerson, M., González-Donoso, J. M., Romero, O. E., Linares, D., Sakamoto, T., Gallego-Torres, D., Rueda Ruiz, J. L., Ortega-Huertas, M., and Perez Claros, J. A.: Detrital input, productivity fluctuations, and water mass circulation in the westernmost Mediterranean Sea since the Last Glacial Maximum, Geochem. Geophy. Geosy., 9, Q11U02, doi:10.1029/2008gc002096, 2008.
Jirikowic, J. L. and Damon, P. E.: The medieval solar activity maximum, Clim. Change, 26,

CPD
7, 635–675, 2011

309–316, doi:10.1007/BF01092421, 1994.
Jones, M. D., Roberts, C. N., Leng, M. J., and Türkes, M.: A high-resolution late Holocene lake isotope record from Turkey and links to North Atlantic and monsoon climate, Geology, 34, 361–364, doi:10.1130/g22407.1, 2006.
Jones, P. D., Osborn, T. J., and Briffa, K. R.: The evolution of climate over the Last Millennium, Science, 292, 662–667, doi:10.1126/science.1059126, 2001.
Kinder, T. H. and Parrilla, G.: Yes, some of the Mediterranean Outflow does come from great depth, J. Geophys. Res., 92, 2901–2906, doi:10.1029/JC092iC03p02901, 1987.
Kisch, H. J.: Illite crystallinity: recommendations on sample preparation, X-ray diffraction settings, and interlaboratory samples, J. Metamorph. Geo., 9, 665–670, doi:10.1111/j.1525-1314.1991.tb00556.x, 1991.
Kolla, V., Biscaye, P. E., and Hanley, A. F.: Distribution of quartz in late Quaternary Atlantic sediments in relation to climate, Quatern. Res., 11, 261–277, doi:10.1016/0033-5894(79)90008-5, 1979.
Lamb, H. H.: The early medieval warm epoch and its sequel, Palaeogeogr., Palaeoclimatol., Palaeoecol., 1, 13–37, doi:10.1016/0031-0182(65)90004-0, 1965.
Macklin, M. G., Benito, G., Gregory, K. J., Johnstone, E., Lewin, J., Michczynska, D. J., Soja, R., Starkel, L., and Thorndycraft, V. R.: Past hydrological events reflected in the Holocene fluvial record of Europe, CATENA, 66, 145–154, doi:10.1016/j.catena.2005.07.015, 2006.
Magny, M.: Holocene climate variability as reflected by mid-European lake-level fluctuations and its probable impact on prehistoric human settlements, Quatern. Int., 113, 65–79, doi:10.1016/S1040-6182(03)00080-6, 2004.
Magny, M., Guiot, J., and Schoellammer, P.: Quantitative reconstruction of Younger Dryas to Mid-Holocene paleoclimates at Le Locle, Swiss Jura, using pollen and lake-level data, Quatern. Res., 56, 170–180, doi:10.1006/qres.2001.2257, 2001.
Magny, M., Miramont, C., and Sivan, O.: Assessment of the impact of climate and anthropogenic factors on Holocene Mediterranean vegetation in Europe on the basis of palaeohydrological records, Palaeogeogr., Palaeoclimatol., Palaeoecol., 186, 47–59, doi:10.1016/S0031-0182(02)00442-X, 2002.
Mangini, A., Blumbach, P., Verdes, P., Spötl, C., Scholz, D., Machel, H., and Mahon, S.: Combined records from a stalagmite from Barbados and from lake sediments in Haiti reveal variable seasonality in the Caribbean between 6.7 and 3 ka BP, Quaternary Sci. Rev., 26, 1332–1343, doi:10.1016/j.quascirev.2007.01.011, 2007.

CPD
7, 635–675, 2011

Martin, J. D.: Using XPowder: A software package for Powder X-Ray diffraction analysis, Granada, Spain, 105 pp., 2004.
Martín-Puertas, C., Jiménez-Espejo, F., Martínez-Ruiz, F., Nieto-Moreno, V., Rodrigo, M., Mata, M. P., and Valero-Garcés, B. L.: Late Holocene climate variability in the southwestern Mediterranean region: an integrated marine and terrestrial geochemical approach, Clim. Past., 6, 807–816, doi:0.5194/cp-6-807-2010, 2010.
Martínez-Ruiz, F., Comas, M. C., and Alonso, B.: Mineral associations and geochemical indicators in upper Miocene to Pleistocene sediments in the Alboran Basin, in: Proceedings of the Ocean Drilling Program, Scientific Results, edited by: Zahn, R., Comas, M. C., and Klaus, A., College Station, TX, 21–36, 1999.
Martínez-Ruiz, F., Paytan, A., Kastner, M., González-Donoso, J. M., Linares, D., Bernasconi, S. M., and Jimenez-Espejo, F. J.: A comparative study of the geochemical and mineralogical characteristics of the S1 sapropel in the western and eastern Mediterranean, Palaeogeogr., Palaeoclimatol., Palaeoecol., 190, 23–37, doi:10.1016/S0031-0182(02)00597-7, 2003.
Masqué, P., Fabres, J., Canals, M., Sanchez-Cabeza, J. A., Sanchez-Vidal, A., Cacho, I., Calafat, A. M., and Bruach, J. M.: Accumulation rates of major constituents of hemipelagic sediments in the deep Alboran Sea: a centennial perspective of sedimentary dynamics, Mar. Geol., 193, 207–233, doi:10.1016/S0025-3227(02)00593-5, 2003.
Masson, V., Vimeux, F., Jouzel, J., Morgan, V., Delmotte, M., Ciais, P., Hammer, C., Johnsen, S., Lipenkov, V. Y., Mosley-Thompson, E., Petit, J.R., Steig, E. J., Stievenard, M., and Vaikmae, R.: Holocene climate variability in Antarctica based on 11 ice-core isotopic records, Quatern. Res., 54, 348–358, doi:10.1006/qres.2000.2172, 2000.
Mayewski, P. A., Rohling, E. E., Curt Stager, J., Karlén, W., Maasch, K. A., David Meeker, L., Meyerson, E. A., Gasse, F., van Kreveld, S., Holmgren, K., Lee-Thorp, J., Rosqvist, G., Rack, F., Staubwasser, M., Schneider, R. R., and Steig, E. J.: Holocene climate variability, Quatern. Res., 62, 243–255, doi:10.1016/j.yqres.2004.07.001, 2004.
McCave, I. N. and Hall, I. R.: Size sorting in marine muds: Processes, pitfalls, and prospects for paleoflow-speed proxies, Geochem. Geophy. Geosy., 7, Q10N05, doi:10.1029/2006gc001284, 2006.
McCave, I. N., Manighetti, B., and Robinson, S. G.: Sortable silt and fine sediment size/composition slicing: parameters for palaeocurrent speed and palaeoceanography, Paleoceanography, 10, 593–610, doi:10.1029/94pa03039, 1995.
McDermott, F., Mattey, D. P., and Hawkesworth, C.: Centennial-scale Holocene climate vari-

CPD
7, 635–675, 2011

ability revealed by a high-resolution speleothem δ^{18}O record from SW Ireland, Science, 294, 1328–1331, doi:10.1126/science.1063678, 2001.
Melki, T., Kallel, N., Jorissen, F. J., Guichard, F., Dennielou, B., Berné, S., Labeyrie, L., and Fontugne, M.: Abrupt climate change, sea surface salinity and paleoproductivity in the western Mediterranean Sea (Gulf of Lion) during the last 28 kyr, Palaeogeogr., Palaeoclimatol., Palaeoecol., 279, 96–113, doi:10.1016/j.palaeo.2009.05.005, 2009.
Millot, C.: Circulation in the Western Mediterranean Sea, J. Mar. Syst., 20, 423–442, doi:10.1016/S0924-7963(98)00078-5, 1999.
Moberg, A., Sonechkin, D. M., Holmgren, K., Datsenko, N. M., and Karlen, W.: Highly variable Northern Hemisphere temperatures reconstructed from low- and high-resolution proxy data, Nature, 433, 613–617, doi:10.1038/nature03265, 2005.
Moreno, A., Cacho, I., Canals, M., Grimalt, J. O., and Sanchez-Vidal, A.: Millennial-scale variability in the productivity signal from the Alboran Sea record, Western Mediterranean Sea, Palaeogeogr., Palaeoclimatol., Palaeoecol., 211, 205–219, doi:10.1016/j.palaeo.2004.05.007, 2004.
Moreno, A., Cacho, I., Canals, M., Grimalt, J. O., Sánchez-Goñi, M. F., Shackleton, N., and Sierro, F. J.: Links between marine and atmospheric processes oscillating on a millennial time-scale. A multi-proxy study of the last 50,000 yr from the Alboran Sea (Western Mediterranean Sea), Quaternary Sci. Rev., 24, 1623–1636, doi:10.1016/j.quascirev.2004.06.018, 2005.
Moulin, C., Lambert, C. E., Dulac, F., and Dayan, U.: Control of atmospheric export of dust from North Africa by the North Atlantic Oscillation, Nature, 387, 691–694, 1997.
O'Brien, S. R., Mayewski, P. A., Meeker, L. D., Meese, D. A., Twickler, M. S., and Whitlow, S. I.: Complexity of Holocene climate as reconstructed from a Greenland ice core, Science, 270, 1962–1964, doi:10.1126/science.270.5244.1962, 1995.
Oksanen J., Kindt R., Legendre P., O'Hara B., Simpson G. L., Solymos P., Stevens M. H. H. and Wagner H.: Vegan: Community Ecology Package, available at: http://cran.r-project.org/web/packages/vegan/index.html (last access: January 2011), R package version 1.15–4, 2009.
Perkins, H., Kinder, T., and Violette, P. L.: The Atlantic inflow in the Western Alboran Sea, J. Phys. Oceanogr., 20, 242–263, 1990.
Reimer, P. J., Baillie, M. G. L., Bard, E., Bayliss, A., Beck, J. W., Blackwell, P. G., Ramsey, C. B., Buck, C. E., Burr, G. S., Edwards, R. L., Friedrich, M., Grootes, P. M., Guilderson, T. P., Hajdas, I., Heaton, T. J., Hogg, A. G., Hughen, K. A., Kaiser, K. F., Kromer, B., McCormac,

CPD
7, 635–675, 2011

F. G., Manning, S. W., Reimer, R. W., Richards, D. A., Southon, J. R., Talamo, S., Turney, C. S. M., van der Plicht, J., and Weyhenmeye, C. E.: INTCAL09 and MARINE09 Radiocarbon age calibration curve, 0–50000 years cal BP, Radiocarbon, 51, 1111–1150, 2009.

Rimbu, N., Lohmann, G., Lorenz, S. J., Kim, J. H., and Schneider, R. R.: Holocene climate variability as derived from alkenone sea surface temperature and coupled ocean-atmosphere model experiments, Clim. Dynam., 23, 215–227, doi:10.1007/s00382-004-0435-8, 2004.

Rodó, X., Baert, E., and Comín, F. A.: Variations in seasonal rainfall in Southern Europe during the present century: relationships with the North Atlantic Oscillation and the El Niño-Southern Oscillation, Clim. Dynam., 13, 275–284, doi:10.1007/s003820050165, 1997.

Rogerson, M., Cacho, I., Jiménez-Espejo, F. J., Reguera, M. I., Sierro, F. J., Martínez-Ruiz, F., Frigola, J., and Canals, M.: A dynamic explanation for the origin of the western Mediterranean organic-rich layers, Geochem. Geophy. Geosy., 9, Q07U01, doi:10.1029/2007GC001936, 2008.

Rohling, E. J., Hayes, A., Mayewski, P. A., and Kucera, M.: Holocene climate variability in the Eastern Mediterranean, and the end of the Bronze Age, in: Forces of Transformation: The end of the Bronze Age in the Mediterranean, edited by: Bachhuber, C. and Roberts, R. G., BANEA Publication Series 1, Oxbow Books, Oxford, 2–5, 2009.

Sánchez-Goñi, M. F., Cacho, I., Turon, J. L., Guiot, J., Sierro, F. J., Peypouquet, J. P., Grimalt, J. O., and Shackleton, N. J.: Synchroneity between marine and terrestrial responses to millennial scale climatic variability during the last glacial period in the Mediterranean region, Clim. Dynam., 19, 95–105, doi:10.1007/s00382-001-0212-x, 2002.

Sierro, F. J., Hodell, D. A., Curtis, J. H., Flores, J. A., Reguera, I., Colmenero-Hidalgo, E., Bárcena, M. A., Grimalt, J. O., Cacho, I., Frigola, J., and Canals, M.: Impact of iceberg melting on Mediterranean thermohaline circulation during Heinrich events, Paleoceanography, 20, PA2019, doi:10.1029/2004pa001051, 2005.

Stein, R., Hefter, J., Grützner, J., Voelker, A., and Naafs, B. D. A.: Variability of surface water characteristics and Heinrich-like events in the Pleistocene midlatitude North Atlantic Ocean: Biomarker and XRD records from IODP Site U1313 (MIS 16-9), Paleoceanography, 24, PA2203, doi:10.1029/2008pa001639, 2009.

Steinhilber, F., Beer, J., and Fröhlich, C.: Total solar irradiance during the Holocene, Geophys. Res. Lett., 36, L19704, doi:10.1029/2009gl040142, 2009.

Stuiver, M. and Reimer, P. J.: Extended C-14 database and revised Calib 3.0 C-14 age calibration program, Radiocarbon, 35, 215–230, 1993.

CPD
7, 635–675, 2011

Sumner, G., Homar, V., and Ramis, C.: Precipitation seasonality in eastern and southern coastal Spain, Int. J. Climatol., 21, 219–247, doi:10.1002/joc.600, 2001.
ten Haven, H. L., de Leeuw, J. W., Schenck, P. A., and Klaver, G. T.: Geochemistry of Mediterranean sediments. Bromine/organic carbon and uranium/organic carbon ratios as indicators for different sources of input and post-depositional oxidation, respectively, Org. Geochem., 13, 255–261, doi:10.1016/0146-6380(88)90044-7, 1988.
Thomson, J., Mercone, D., de Lange, G. J., and van Santvoort, P. J. M.: Review of recent advances in the interpretation of eastern Mediterranean sapropel S1 from geochemical evidence, Mar. Geol., 153, 77–89, doi:10.1016/S0025-3227(98)00089-9, 1999.
Trigo, R. M., Osborn, T. J., and Corte-Real, J. M.: The North Atlantic Oscillation influence on Europe: climate impacts and associated physical mechanisms, Clim. Res., 20, 9–17, 2002.
Trouet, V., Esper, J., Graham, N. E., Baker, A., Scourse, J. D., and Frank, D. C.: Persistent positive North Atlantic Oscillation mode dominated the Medieval Climate Anomaly, Science, 324, 78–80, doi:10.1126/science.1166349, 2009.
Turney, C. S. M. and Palmer, J. G.: Does the El Niño-Southern Oscillation control the interhemispheric radiocarbon offset?, Quatern. Res., 67, 174–180, doi:10.1016/j.yqres.2006.08.008, 2007.
Van der Weijden, C. H.: Pitfalls of normalization of marine geochemical data using a common divisor, Mar. Geol., 184, 167–187, doi:10.1016/S0025-3227(01)00297-3, 2002.
van Geel, B., Raspopov, O. M., Renssen, H., van der Plicht, J., Dergachev, V. A., and Meijer, H. A. J.: The role of solar forcing upon climate change, Quaternary Sci. Rev., 18, 331–338, doi:10.1016/S0277-3791(98)00088-2, 1999.
Voelker, A. H. L., Lebreiro, S. M., Schönfeld, J., Cacho, I., Erlenkeuser, H., and Abrantes, F.: Mediterranean outflow strengthening during northern hemisphere coolings: A salt source for the glacial Atlantic?, Earth Planet. Sc. Lett., 245, 39–55, doi:10.1016/j.epsl.2006.03.014, 2006.
Wanner, H., Bronnimann, S., Casty, C., Gyalistras, D., Luterbacher, J., Schmutz, C., Stephenson, D. B., and Xoplaki, E.: North Atlantic Oscillation – Concepts and studies, Surv. Geophys., 22, 321–382, doi:10.1023/A:1014217317898, 2001.
Wanner, H., Beer, J., Bütikofer, J., Crowley, T. J., Cubasch, U., Flückiger, J., Goosse, H., Grosjean, M., Joos, F., Kaplan, J. O., Küttel, M., Müller, S. A., Prentice, I. C., Solomina, O., Stocker, T. F., Tarasov, P., Wagner, M., and Widmann, M.: Mid- to Late Holocene climate change: an overview, Quaternary Sci. Rev., 27, 1791–1828,

CPD
7, 635–675, 2011

doi:10.1016/j.quascirev.2008.06.013, 2008.
Willard, D. A., Bernhardt, C. E., Korejwo, D. A., and Meyers, S. R.: Impact of millennial-scale Holocene climate variability on eastern North American terrestrial ecosystems: pollen-based climatic reconstruction, Global Planet. Change, 47, 17–35, doi:10.1016/j.gloplacha.2004.11.017, 2005.
Ziegler, M., Jilbert, T., de Lange, G. J., Lourens, L. J., and Reichart, G.J.: Bromine counts from XRF scanning as an estimate of the marine organic carbon content of sediment cores, Geochem. Geophy. Geosy., 9, Q05009, doi:10.1029/2007gc001932, 2008.

CPD
7, 635–675, 2011

Table 1. Radiocarbon dates and calibrated ages for cores 305G and 306G.

Laboratory code	Core	Core depth (cm)	Conventional radiocarbon age (B.P.)	Calibrated age 2σ (cal. B.P.)
Poz-37150	305G	6–7	1520 ± 30	1070 ± 93
CNA567	305G	8–9	1795 ± 40	1346 ± 88
CNA304	305G	19–20	2320 ± 45	1942 ± 124
Poz-37151	305G	25–26	2335 ± 30	1956 ± 94
CNA305	305G	29–30	2870 ± 45	2613 ± 126
Poz-37152	306G	6–7	1130 ± 35	690.5 ± 63.5
CNA306	306G	9–10	1610 ± 45	1164 ± 102
CNA307	306G	19–20	2200 ± 60	1784 ± 146
Poz-37153	306G	25–26	2645 ± 35	2350 ± 105
CNA308	306G	29–30	3160 ± 45	2959 ± 146

CPD
7, 635–675, 2011

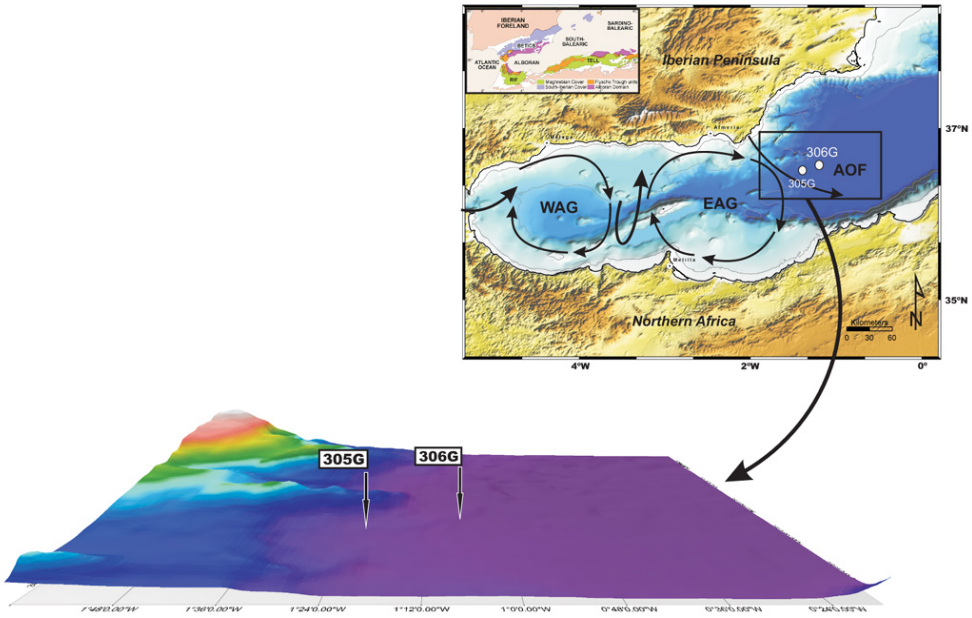

Fig. 1. Site setting of the studied cores in the west Algerian-Balearic basin **(a)** and bathymetric map showing the main physiographic features of the area under study **(b)**. WAG: Western Alboran gyre, EAG: Eastern Alboran gyre, AOF: Almería-Orán Front.

CPD
7, 635–675, 2011

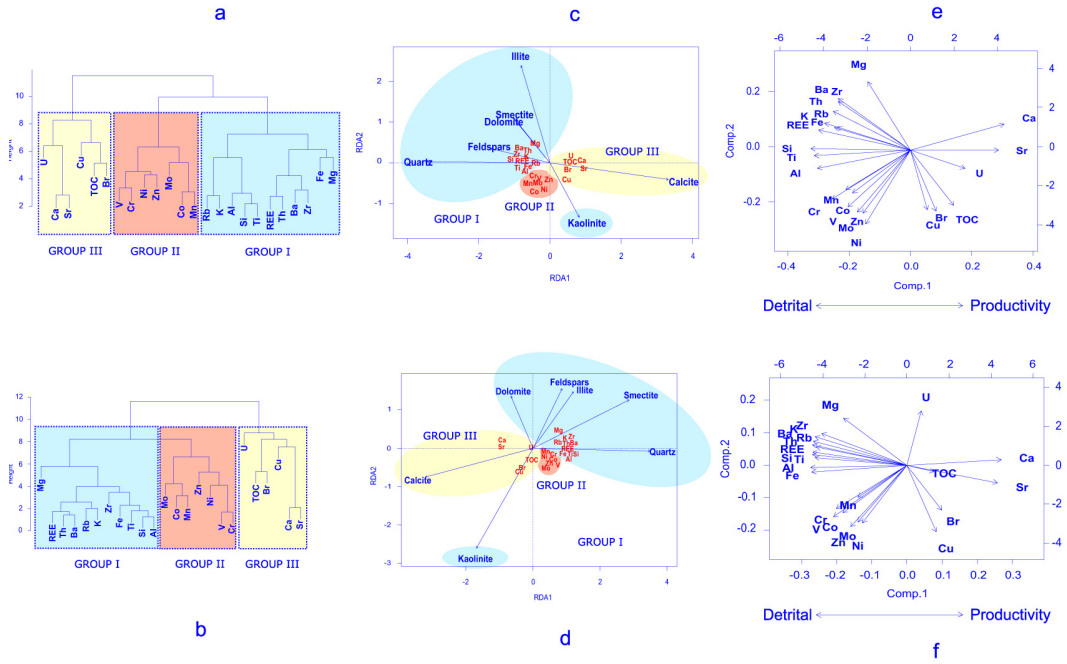

Fig. 2. Statistical treatment of data from both sites. Cluster analyses of the geochemical data for sites 305G **(a)** and 306G **(b)**, showing three main geochemical families in accordance to their affinity and origin. Redundancy analyses (RDA) biplots displaying the relationship between the chemical elements and associated mineral phases for sites 305G **(c)** and 306G **(d)**. Light yellow, orange and blue circles indicate Group I, II or III, respectively. Biplots showing the first and the second eigenvector of the Principal Component Analysis (PCA) for sites 305G **(e)** and 306G **(f)**.

CPD
7, 635–675, 2011

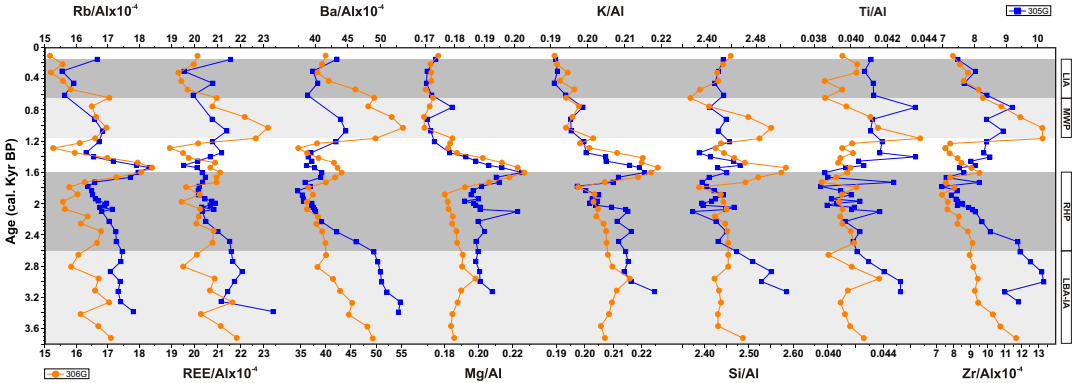

Fig. 3. Age-depth profile of detrital proxies (Rb/Al and Ba/Al $\times 10^{-4}$ ratios, Si/Al, Ti/Al, Mg/Al, and K/Al ratios) for site 305G (blue squares) and site 306G (orange circles). Light grey bars indicate dry periods (LIA: Little Ice Age, LBA-IA: Late Bronze Age-Iron Age); dark grey bars indicate humid periods (MWP: Medieval Warm Period, RHP: Roman Humid Period).

CPD
7, 635–675, 2011

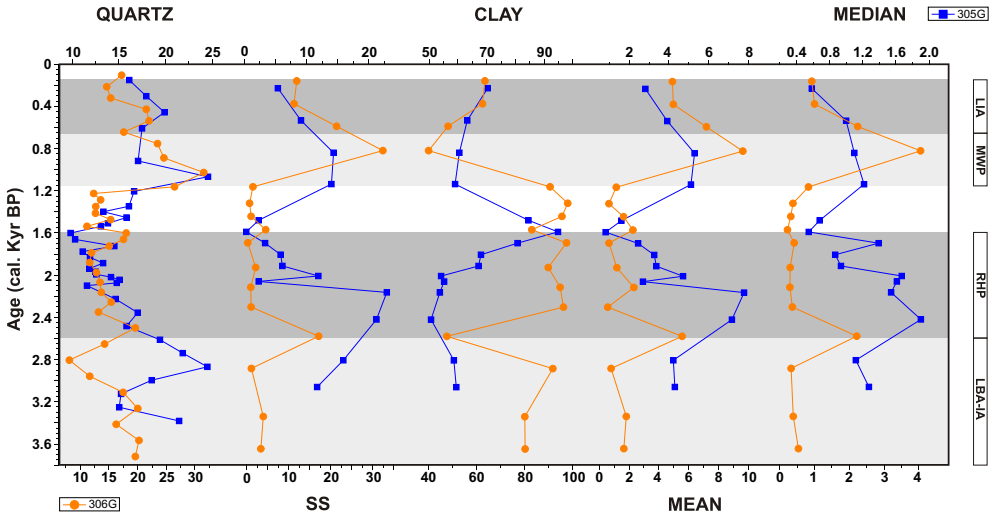

Fig. 4. Age-depth profile of grain size distribution: mean, median, SS (%), clay (%) and quartz content (%) for site 305G (blue squares) and site 306G (orange circles). Light grey bars indicate dry periods (LIA: Little Ice Age, LBA-IA: Late Bronze Age-Iron Age); dark grey bars indicate humid periods (MWP: Medieval Warm Period, RHP: Roman Humid Period).

CPD
7, 635–675, 2011

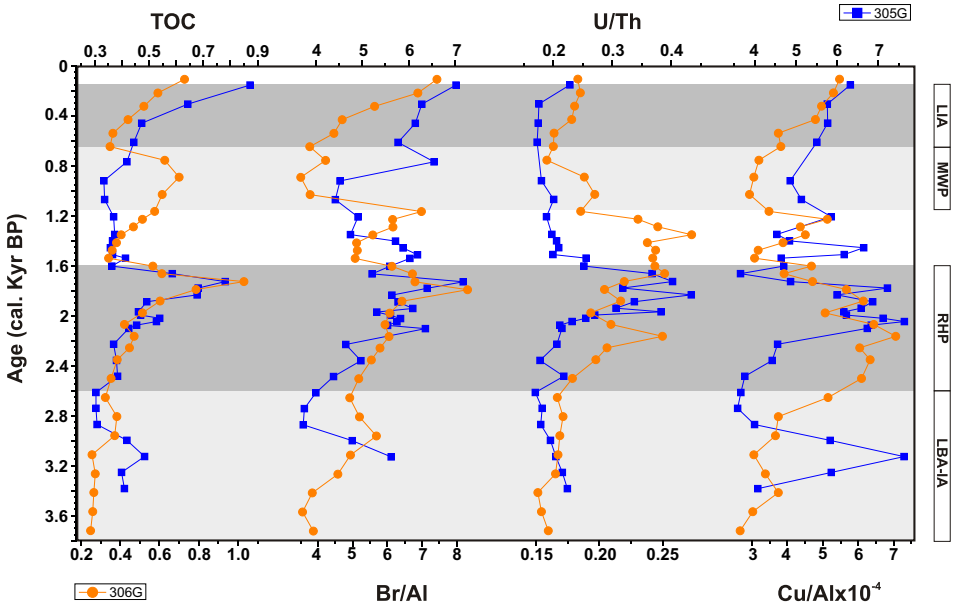

Fig. 5. Age-depth profile of paleo-productivity indicators (Cu/Al × 10^{-4}, TOC, Br/Al and U/Th) for site 305G (blue squares) and site 306G (orange circles). Light grey bars indicate dry periods (LIA: Little Ice Age, LBA-IA: Late Bronze Age-Iron Age); dark grey bars indicate humid periods (MWP: Medieval Warm Period, RHP: Roman Humid Period).

CPD
7, 635–675, 2011

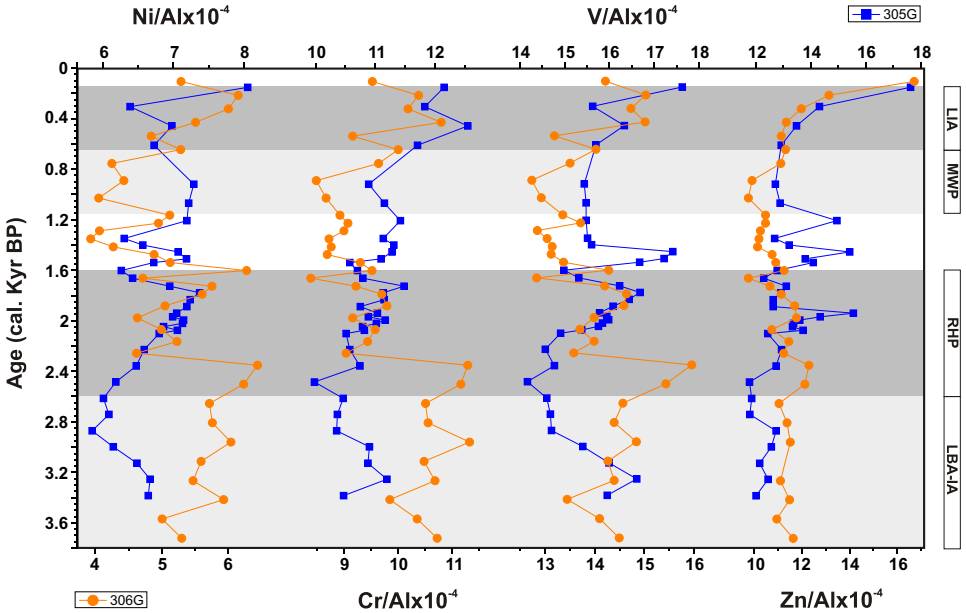

Fig. 6. Age-depth profile of redox proxies (V/Al, Cr/Al, Ni/Al and Zn/Al × 10^{-4} ratios) for site 305G (blue squares) and site 306G (orange circles). Light grey bars indicate dry periods (LIA: Little Ice Age, LBA-IA: Late Bronze Age-Iron Age); dark grey bars indicate humid periods (MWP: Medieval Warm Period, RHP: Roman Humid Period).

CPD
7, 635–675, 2011

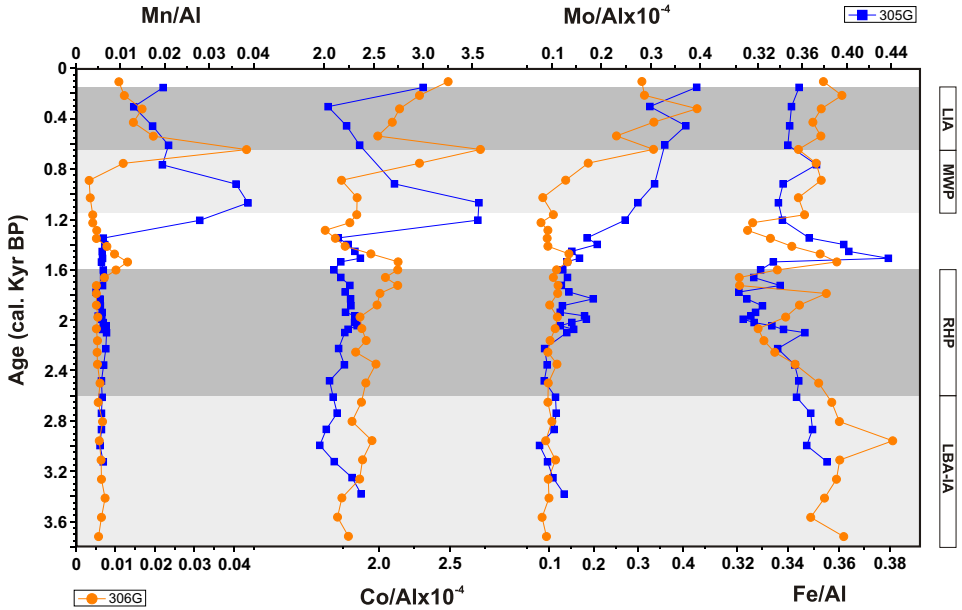

Fig. 7. Age-depth profile of post-depositional proxies (Co/Al and Mo/Al $\times 10^{-4}$, Mn/Al and Fe/Al) for site 305G (blue squares) and site 306G (orange circles). Light grey bars indicate dry periods (LIA: Little Ice Age, LBA-IA: Late Bronze Age-Iron Age); dark grey bars indicate humid periods (MWP: Medieval Warm Period, RHP: Roman Humid Period).

CPD
7, 635–675, 2011

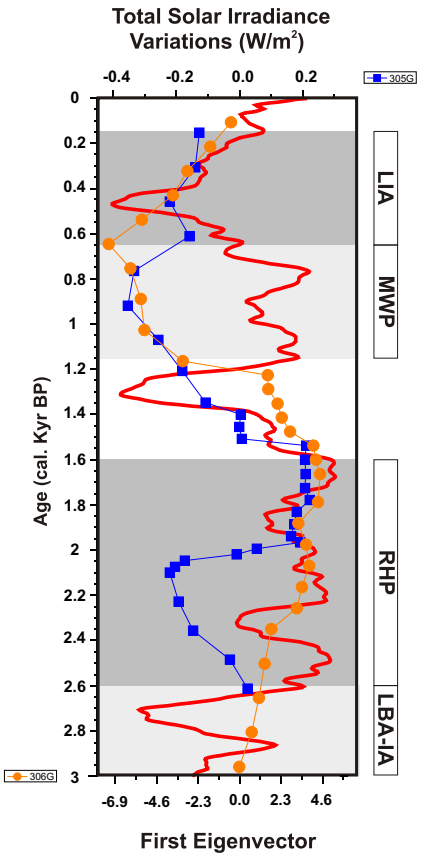

Fig. 8. First eigenvector of sites 305G (blue squares) and 306G (orange circles) compared with the 30 year-moving average of total solar irradiance variations (W m^{-2}) during the last 4000 yr (red line) (Steinhilber et al., 2009). Light grey bars indicate dry periods (LIA: Little Ice Age, LBA-IA: Late Bronze Age-Iron Age); dark grey bars indicate humid periods (MWP: Medieval Warm Period, RHP: Roman Humid Period).

CPD
7, 635–675, 2011